Supplementary Materials

Synthesis, Spectroscopic Characterization and Photophysical Studies of Heteroleptic Silver Complexes bearing 2,9-Bis(styryl)-1,10-phenanthroline ligands and Bis [(2-diphenylphosphino) phenyl] ether

Dimitrios Glykos [1], Athanassios C. Tsipis [1], John C. Plakatouras [1,2] and Gerasimos Malandrinos [1,*]

[1] Laboratory of Inorganic Chemistry, Department of Chemistry, University of Ioannina, 451 10 Ioannina, Greece; d.glykos@uoi.gr (D.G.); iplakatu@uoi.gr (J.C.P.)
[2] Institute of Materials Science and Computing, University Research Center of Ioannina, 451 10 Ioannina, Greece
* Correspondence: gmalandr@uoi.gr

TABLE OF CONTENTS

Figure S17. 3D contour plots of the MOs involved in the electronic excitations giving rise to the two bands appearing in the simulated absorption spectra of **2** calculated at the PBE0/LANL2TZ(Ag)U6-31G(d,p) level of theory in DCM solvent.

Figure S18. 3D contour plots of the MOs involved in the electronic excitations giving rise to the two bands appearing in the simulated absorption spectra of **3** calculated at the PBE0/LANL2TZ(Ag)U6-31G(d,p) level of theory in DCM solvent.

Figure S19. HR-ESI-MS spectrum of the fragment $[AgL]^+$ **1** (top) and theoretical spectrum.

Figure S20. HR-ESI-MS spectrum of the fragment $[AgL]^+$ **2** (top) and theoretical spectrum.

Figure S21. HR-ESI-MS spectrum of the fragment $[AgL]^+$ **3** (top) and theoretical spectrum.

Figure S22. HR-ESI-MS spectrum of the fragment $[L2+H^+]^+$ (top) and theoretical spectrum.

Figure S23. HR-ESI-MS spectrum of the fragment $[L3+H^+]^+$ (top) and theoretical spectrum.

Experimental.

Synthesis of Ligands

General procedure for the synthesis of compounds L2 and L3: Potassium tert-butoxide (486 mg, 3.5 mmol) was slowly added to a solution of the appropriate 4-substituted benzaldehyde derivative (2.2 mmol) and neocuproine hemihydrate (1.0 mmol) in anhydrous DMF (5 mL). The mixture was stirred for 4-6 hours at 50°C, and the reaction progress was monitored by TLC. The reaction mixture was quenched by the addition of water, and the residue obtained was collected by filtration, dissolved in CH_2Cl_2, and washed with an aqueous K_2CO_3 solution. After the removal of the solvent, the crude product was recrystallized from dichloromethane/cyclohexane.

2,9-bis((E)-4-methylthiostyryl)-1,10-phenanthroline (L2): orange solid. Yield 50%. ^{1}H NMR (500 MHz, $CDCl_3$) (ppm): 8.23 (d, *J* = 8.4 Hz, 2H); 7.94 (d, *J* = 8.4 Hz, 2H); 7.77 (d, J = 16.1 Hz, 4H); 7.75 (s, 2H); 7.69 (d, J = 16.1 Hz, 4H); 7.64 (d, *J* = 8.4 Hz, 4H); 7.32 (d, *J* = 8.4 Hz, 4H); 2.56 (s, 6H).

HR ESI-MS: *m*/*z* = 477.1454 for [**L2**+H^+]$^+$ (Figure S22).

2,9-bis((E)-4-diethylaminostyryl)-1,10-phenanthroline (L3): orange solid. Yield 62%. ^{1}H NMR (500 MHz, $CDCl_3$) (ppm): 8.16 (d, *J* = 8.5 Hz, 2H); 7.90 (d, *J* = 8.6 Hz, 2H); 7.72 (d, J = 16.3 Hz, 4H); 7.68 (s, 2H); 7.60 (d, *J* = 8.6 Hz, 4H); 7.54 (d, J = 16.3 Hz, 4H); 6.73 (d, *J* = 8.6 Hz, 4H); 3.45 (q, *J* = 7.1 Hz, 8H); 1.24 (t, *J* = 7.1 Hz, 12H).

HR ESI-MS: *m*/*z* = 527.3169 for [**L3**+H^+]$^+$ (Figure S23).

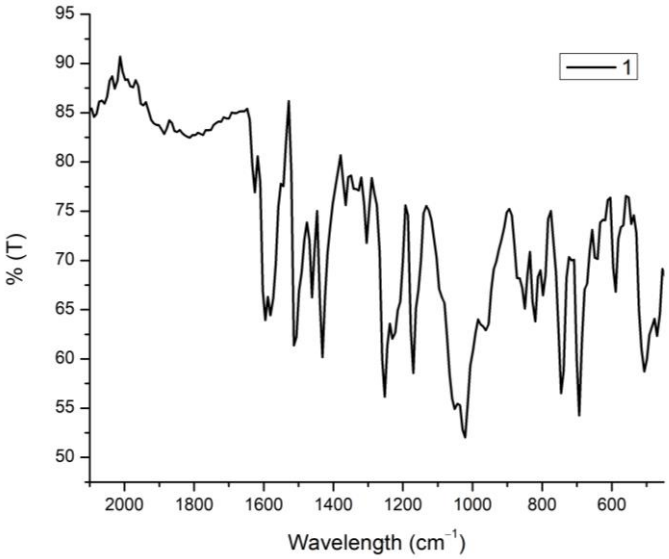

Figure S1. ATR-IR spectrum of complex **1**.

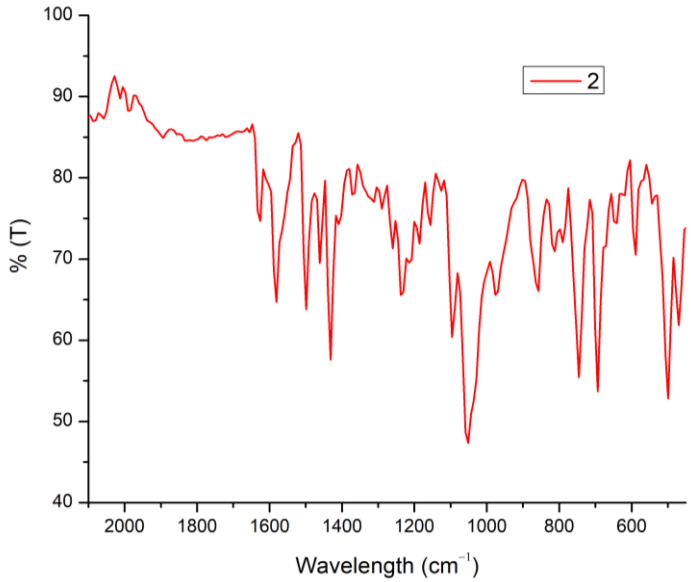

Figure S2. ATR-IR spectrum of complex **2**.

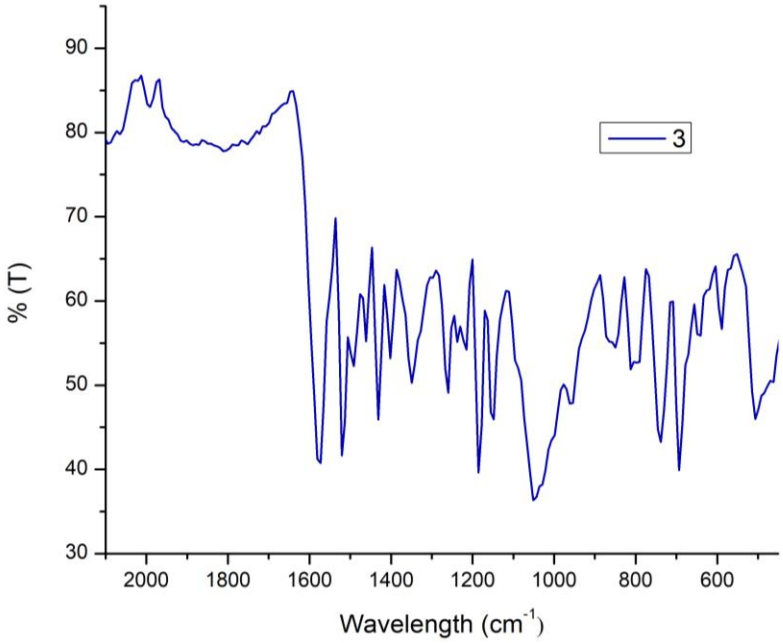

Figure S3. ATR-IR spectrum of complex **3**.

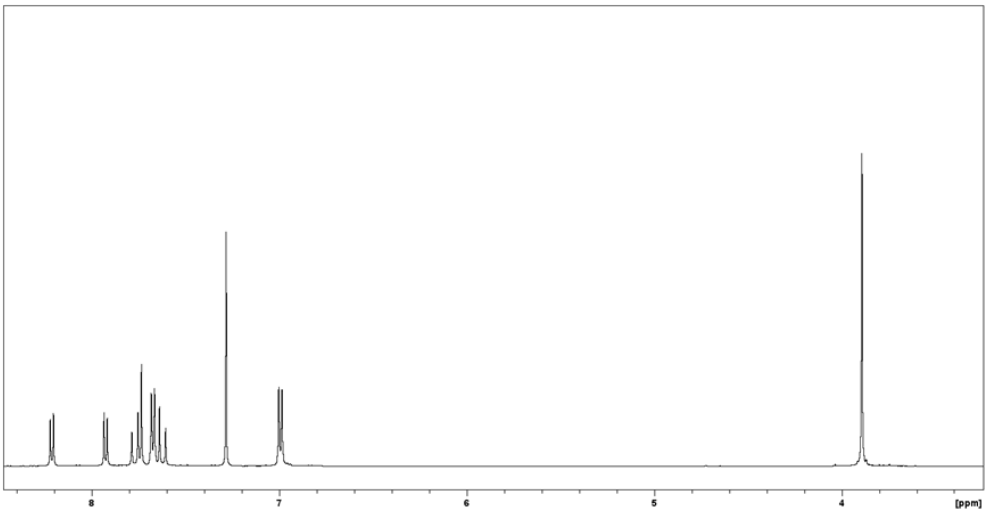

Figure S4. ^{1}H-NMR spectrum of L2 (500 MHz, $CDCl_3$, 298K).

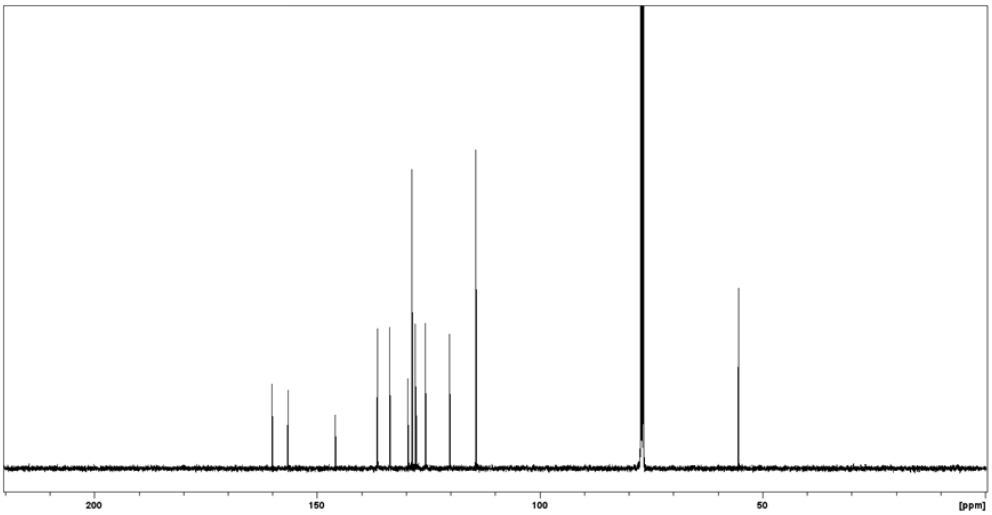

Figure S5. ^{13}C-NMR spectrum of L2 (500 MHz, $CDCl_3$, 298K).

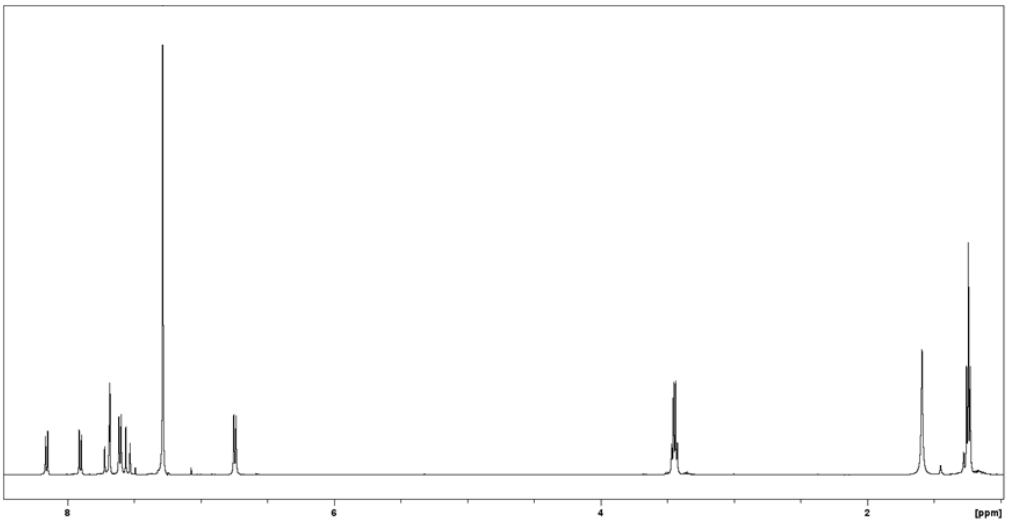

Figure S6. ^{1}H-NMR spectrum of L3 (500 MHz, $CDCl_3$, 298K).

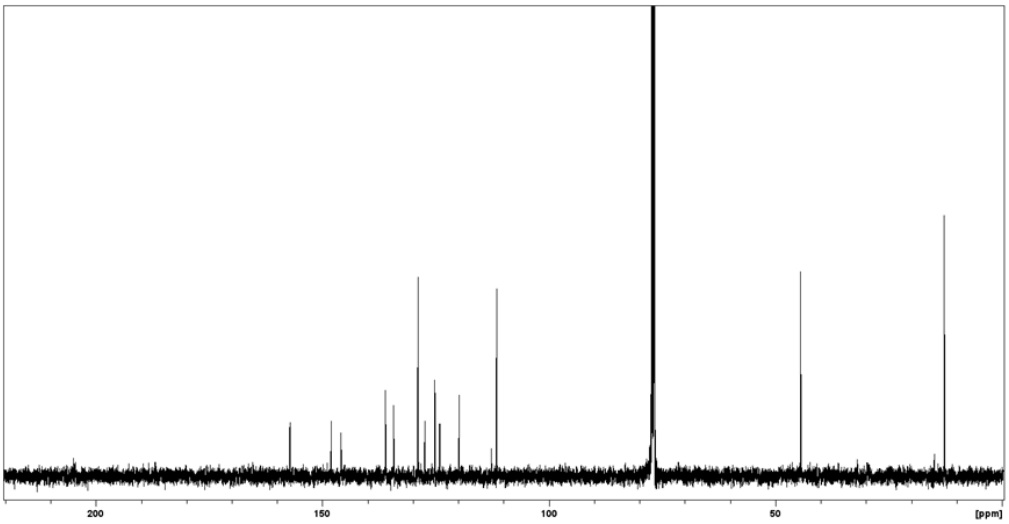

Figure S7. ^{13}C-NMR spectrum of L3 (500 MHz, $CDCl_3$, 298K).

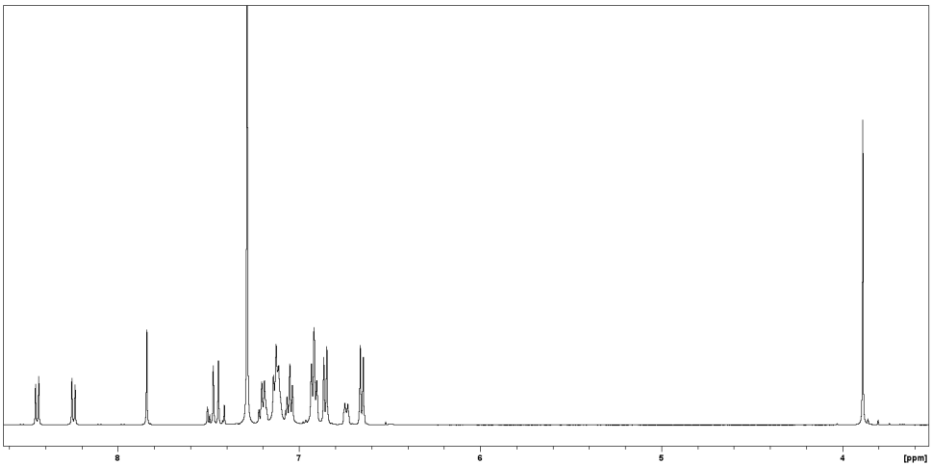

Figure S8. ^{1}H-NMR spectrum of **1** (500 MHz, $CDCl_3$, 298K).

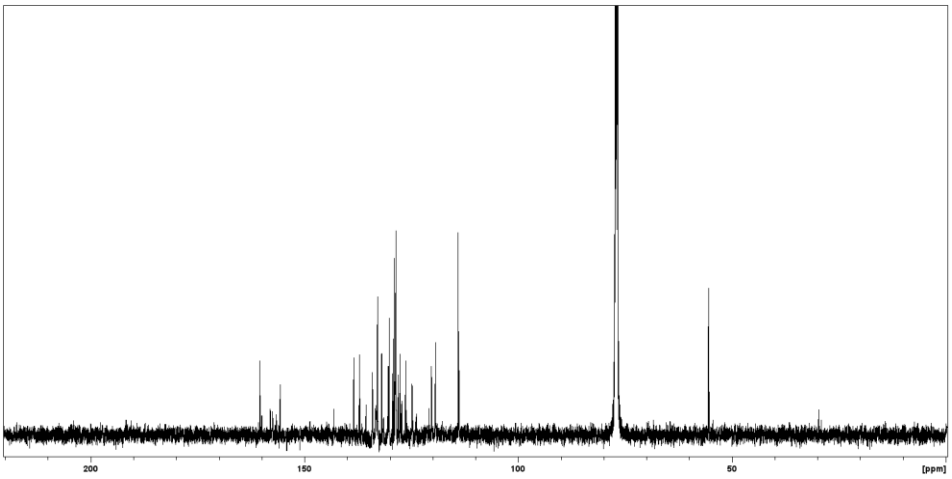

Figure S9. ^{13}C-NMR spectrum of **1** (500 MHz, $CDCl_3$, 298K).

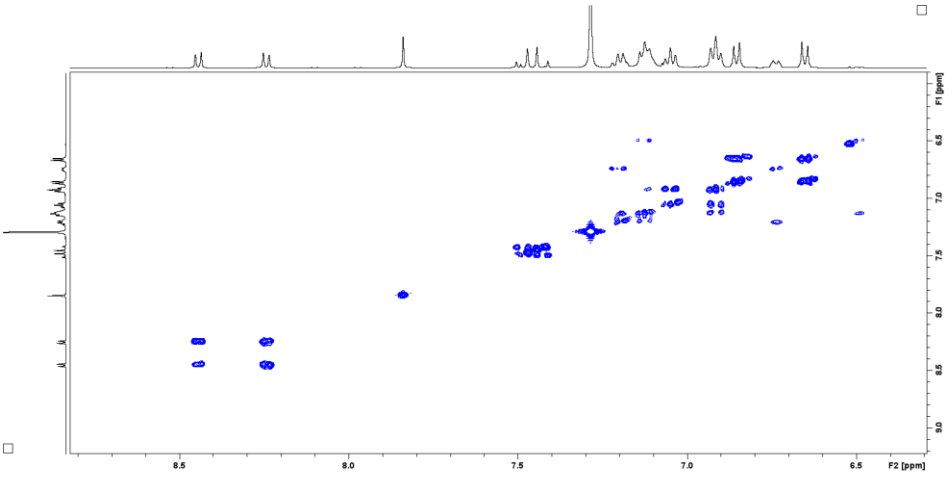

Figure S10. ^{1}H-^{1}H COSY NMR spectrum of **1** (500 MHz, $CDCl_3$, 298K).

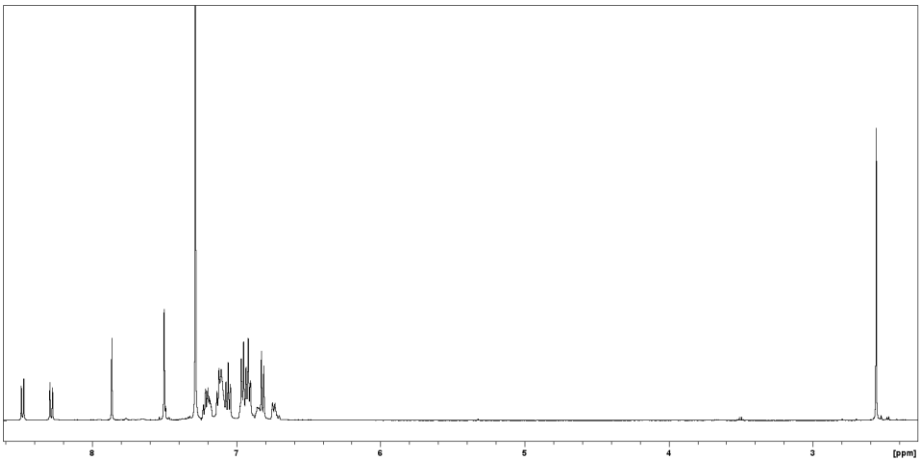

Figure S11. ^{1}H-NMR spectrum of **2** (500 MHz, $CDCl_3$, 298K).

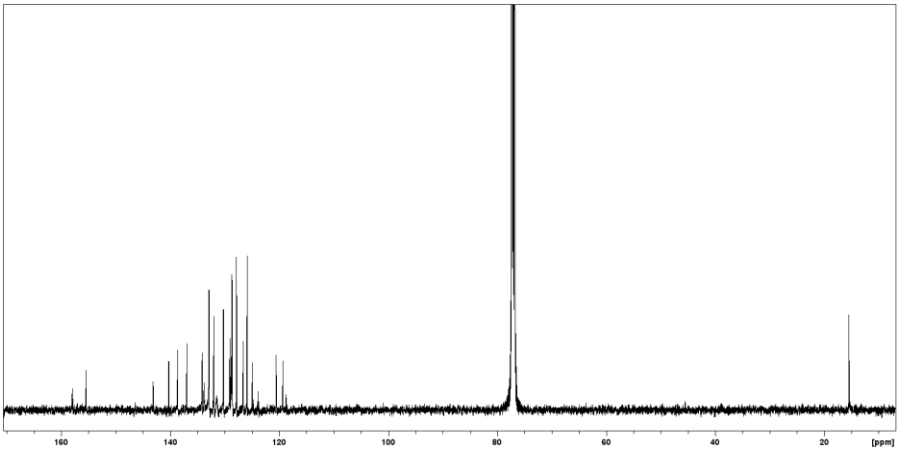

Figure S12. ^{13}C-NMR spectrum of **2** (500 MHz, $CDCl_3$, 298K) .

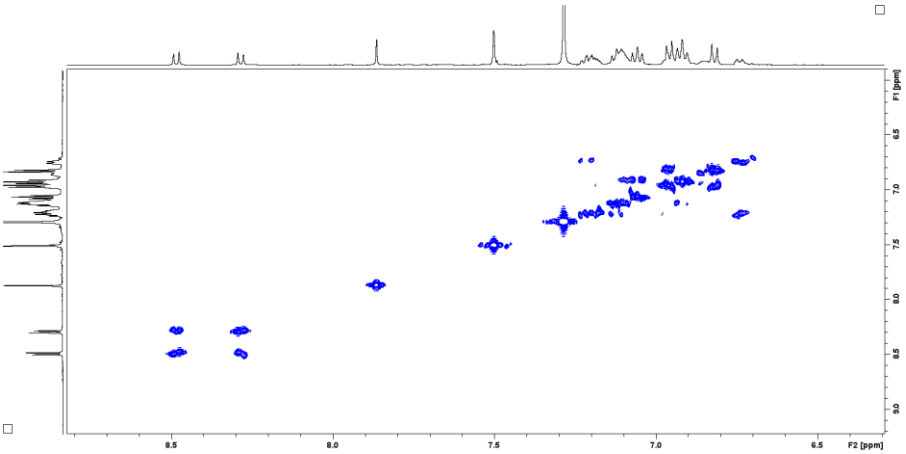

Figure S13. ^{1}H-^{1}H COSY NMR spectrum of **2** (500 MHz, $CDCl_3$, 298K).

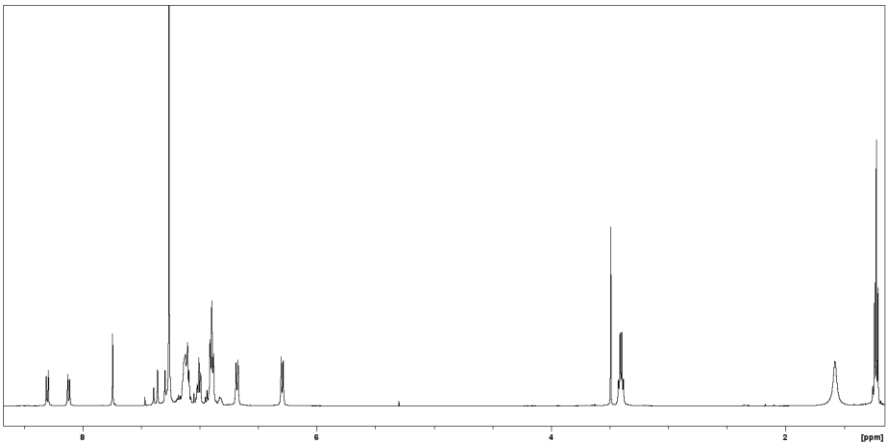

Figure S14. ^{1}H-NMR spectrum of **3** (500 MHz, $CDCl_3$, 298K).

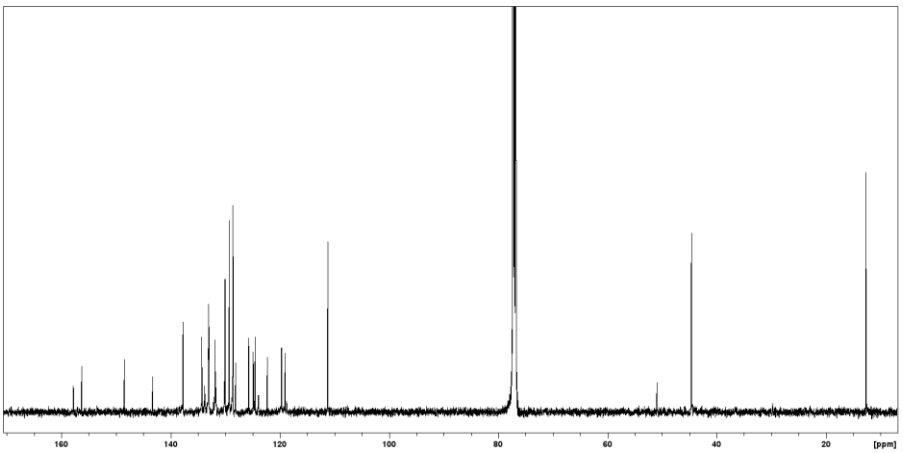

Figure S15. ^{13}C-NMR spectrum of **3** (500 MHz, $CDCl_3$, 298K).

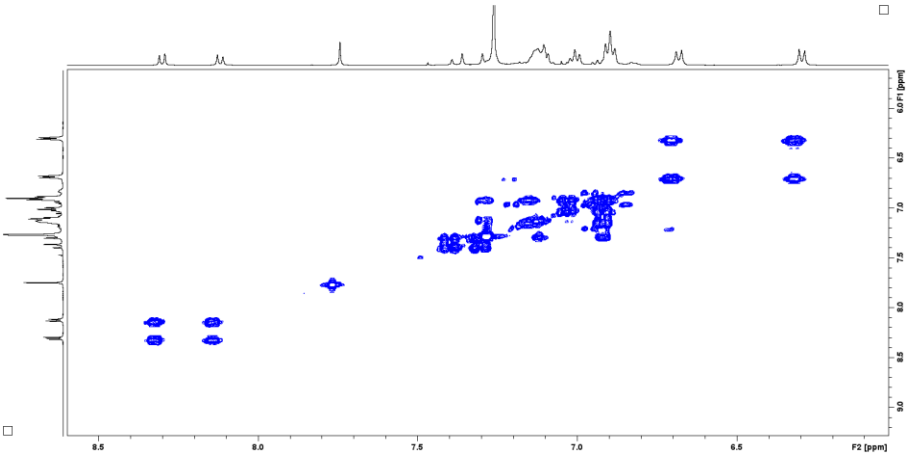

Figure S16. ^{1}H-^{1}H COSY NMR spectrum of **3** (500 MHz, $CDCl_3$, 298K).

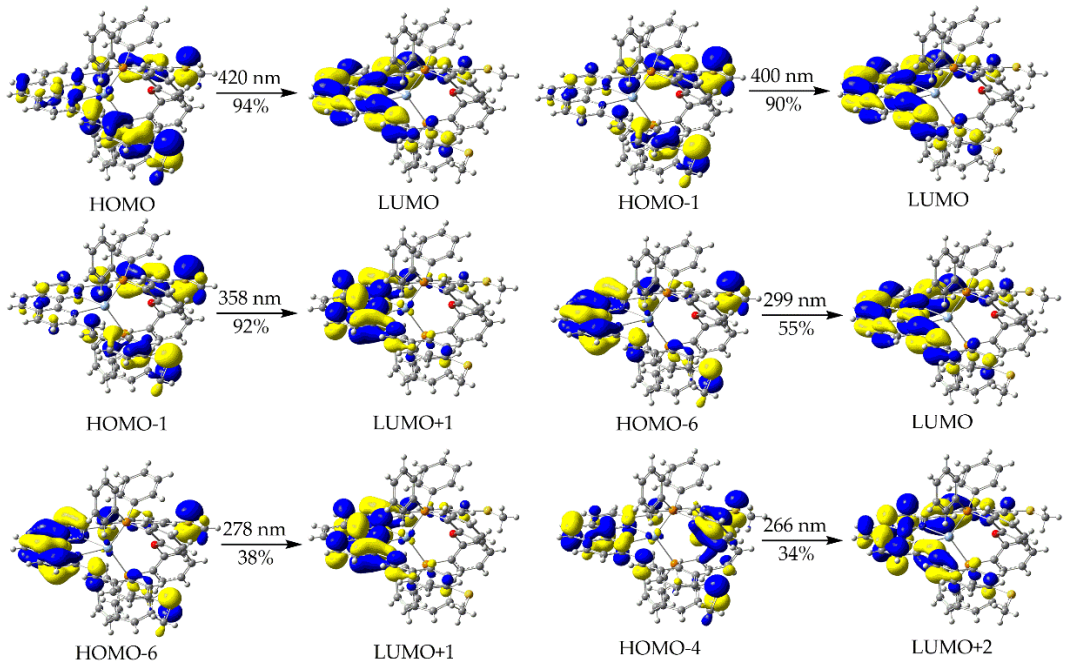

Figure S17. 3D contour plots of the MOs involved in the electronic excitations giving rise to the two bands appearing in the simulated absorption spectra of **2** calculated at the PBE0/LANL2TZ(Ag)U6-31G(d,p) level of theory in DCM solvent.

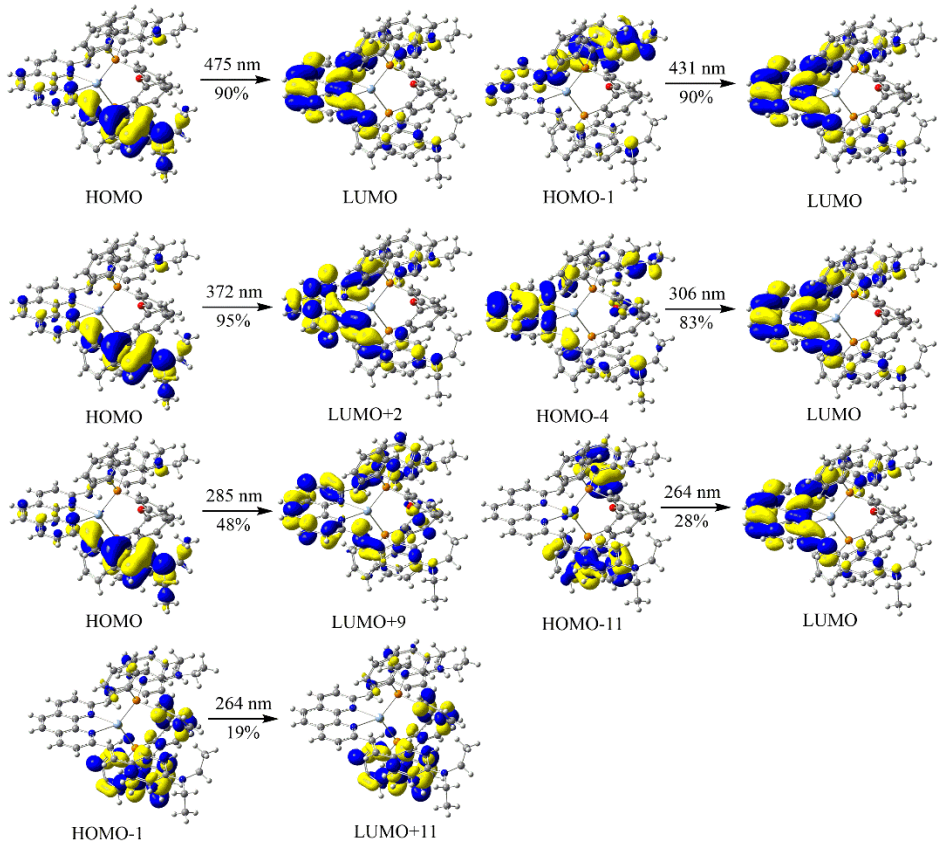

Figure S18. 3D contour plots of the MOs involved in the electronic excitations giving rise to the two bands appearing in the simulated absorption spectra of **3** calculated at the PBE0/LANL2TZ(Ag)U6-31G(d,p) level of theory in DCM solvent.

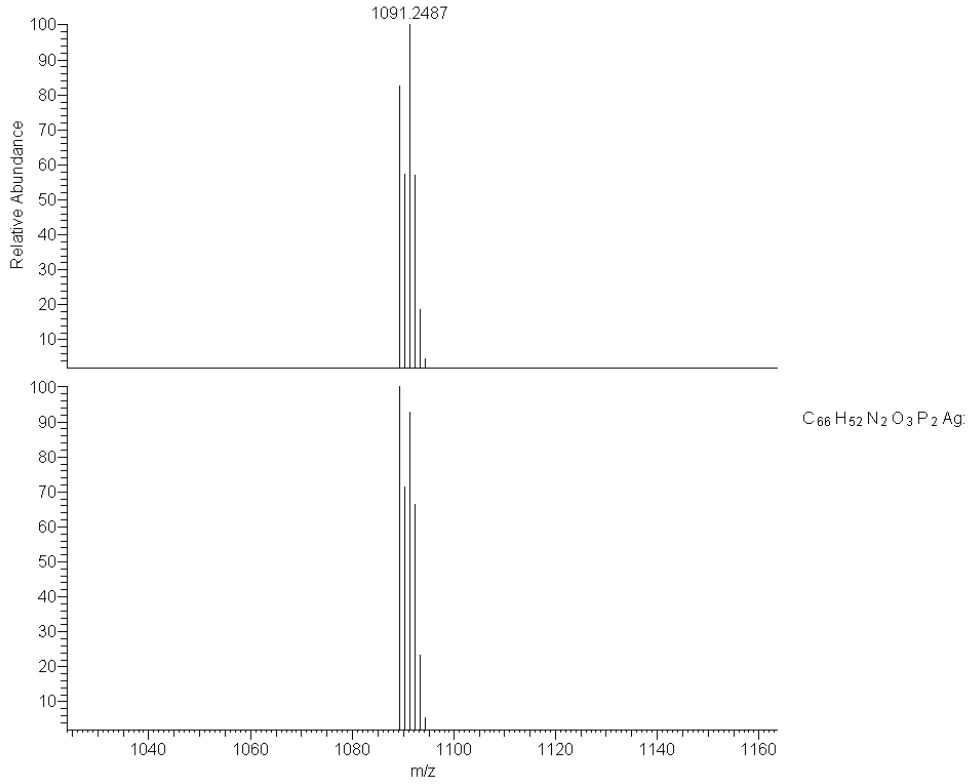

Figure S19. HR-ESI-MS spectrum of the fragment $[AgL]^+$ **1** (top) and theoretical spectrum.

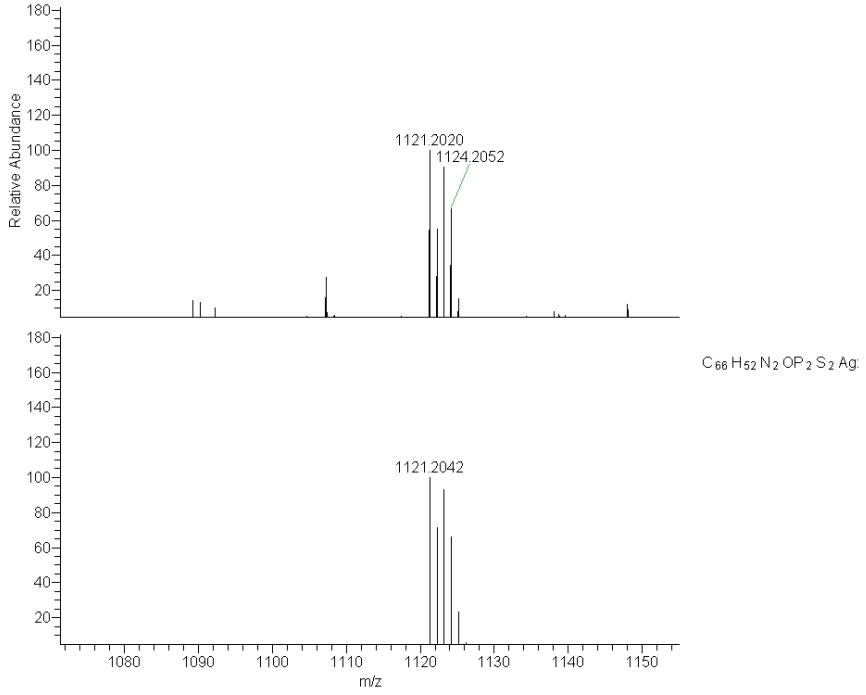

Figure S20. HR-ESI-MS spectrum of the fragment $[AgL]^+$ **2** (top) and theoretical spectrum.

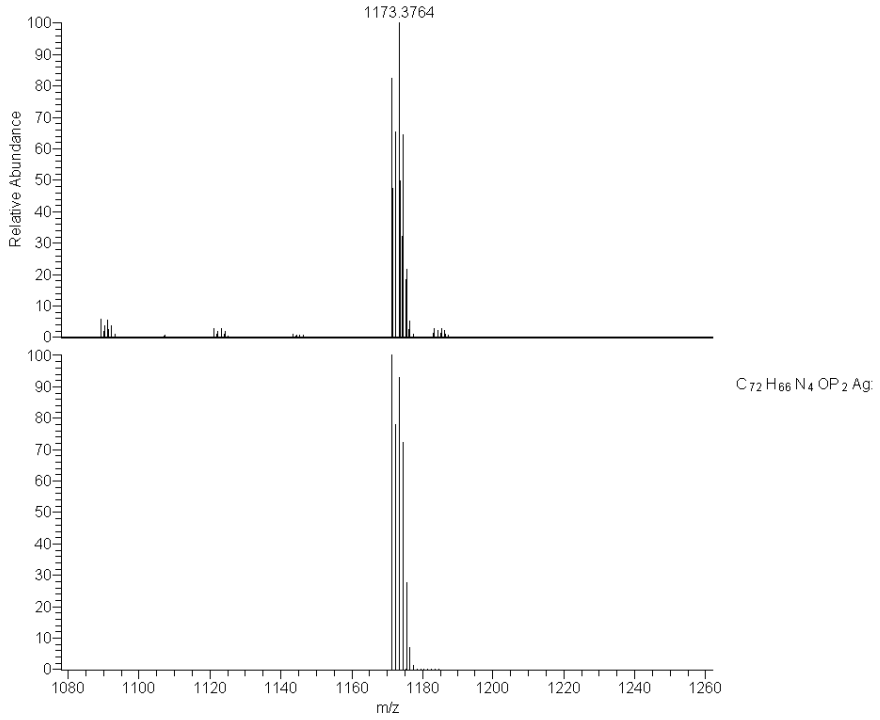

Figure S21. HR-ESI-MS spectrum of the fragment $[AgL]^+$ **3** (top) and theoretical spectrum.

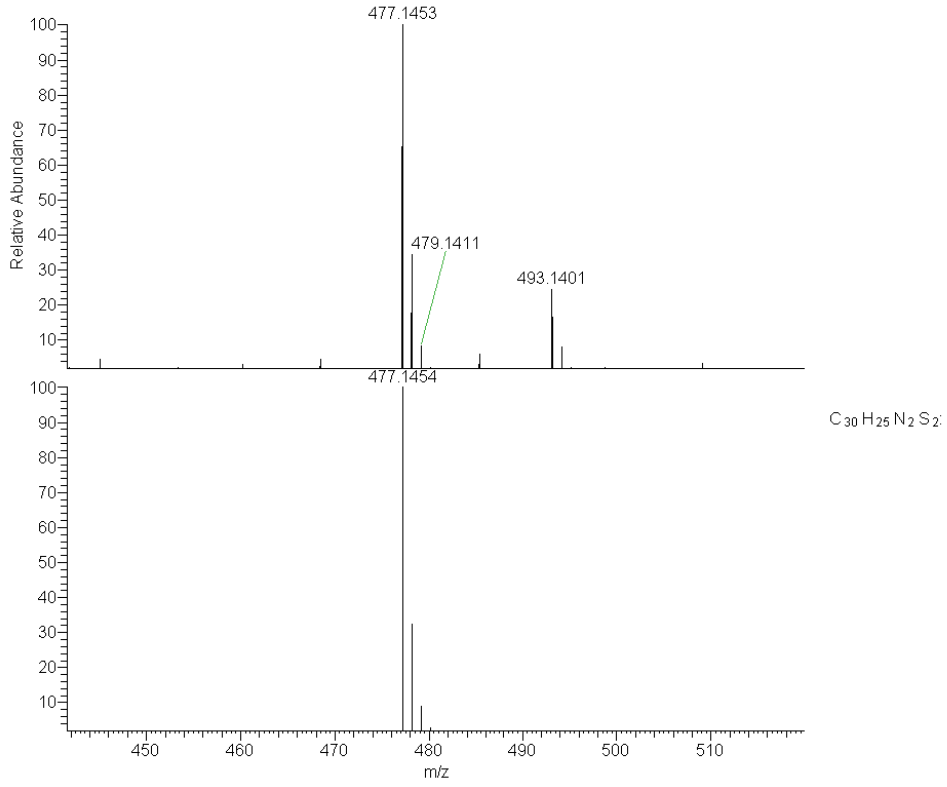

Figure S22. HR-ESI-MS spectrum of the fragment $[L2+H^+]^+$ (top) and theoretical spectrum.

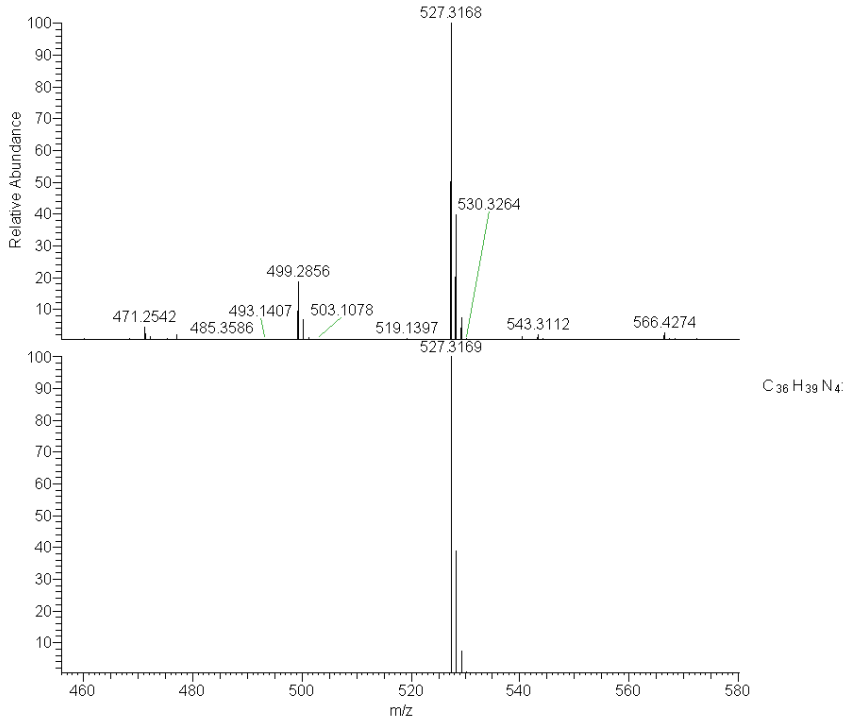

Figure S23. HR-ESI-MS spectrum of the fragment $[L3+H^+]^+$ (top) and theoretical spectrum.